Journal of Sound and Vibration (2002) **253**(3), 687–709
doi:10.1006/jsvi.2001.4075, available online at http://www.idealibrary.com on IDEAL®

TOPOLOGY DESIGN OF STRUCTURES SUBJECTED TO PERIODIC LOADING

C. S. Jog

Facility for Research in Technical Acoustics (*FRITA*), *Department of Mechanical Engineering*, *Indian Institute of Science*, *Bangalore* 560012, *India*. *E-mail*: *jogc@mecheng.iisc.ernet.in*

(*Received* 25 *May* 2001, *and in final form* 3 *October* 2001)

Although a lot of attention in the topology optimization literature has focused on the optimization of eigenfrequencies in free vibration problems, relatively little work has been done on the optimization of structures subjected to periodic loading. In this paper, we propose two measures, one global and the other local, for the minimization of vibrations of structures subjected to periodic loading. The global measure which we term as the "dynamic compliance" reduces the vibrations in an overall sense, and thus has important implications from the viewpoint of reducing the noise radiated from a structure, while the local measure reduces the vibrations at a user-defined point. Both measures bring about a reduction in the vibration level by moving the natural frequencies which contribute most significantly to the measures, away from the driving frequencies, although, as expected, in different ways. Quite surprisingly, the structure of the dynamic compliance optimization problem turns out to be very similar to the structure of the static compliance optimization problem. The availability of analytical sensitivities results in an efficient algorithm for both measures. We show the effectiveness of the measures by presenting some numerical examples.

1. INTRODUCTION

Topology optimization, which involves distributing a given amount of material in a domain subjected to certain loading and boundary conditions, in a configuration of macroscopic solid and void regions so as to optimize a given performance functional, has been applied extensively for static problems (see, for example, [1–4]). Typically, the functional that is optimized is the compliance which is the work done by the loads; minimizing the compliance corresponds to maximizing the stiffness of the structure.

For dynamic problems, attention has been focused primarily on the optimization of natural frequencies of vibrating structures (e.g., [5–9]). The problem of minimization of vibrations of structures subjected to periodic loading is also of great importance since the major source of vibration, and hence noise, in a machine is a periodic force due to rotating components. Thus, the reduction of vibration of structures subjected to periodic loading could have great practical implications in reducing the noise radiated in many practical situations, ranging from portable electric tools and washing machines to cars and ships.

Ma *et al.* [9] briefly discuss the problem of reducing the vibrations of structures subjected to periodic loading. They formulate a "dynamic compliance", the minimization of which results in reduced vibration of the structure. However, one of the shortcomings of this proposed measure is that, unlike the static compliance, it is not a positive-definite measure. Thus, if the driving frequency of the load is slightly higher than the fundamental frequency,

0022-460X/02/$35.00

say, then their dynamic compliance becomes negative (see equation (30) in reference [9]), and minimization of this function drives the system towards resonance instead of away from it. They also ignore damping in their work. To remedy these shortcomings, we propose a new definition of dynamic compliance for structures subjected to periodic loading, and show that it is a positive-definite measure in the sense that it is positive in the presence of vibrations, and is zero if and only if the structure is static. Thus, minimizing the dynamic compliance drives the structure towards the static state.

Although the dynamic compliance is useful in reducing vibrations in a global or overall sense, in certain applications, it is desirable to minimize the frequency response amplitude at a given point in the structure, although it might well be at the expense of increasing the amplitudes at other points in the structure, e.g., it is desirable to minimize the amplitude of vibration at the sonar compartment of a ship. Although several works deal with the minimization of frequency response amplitudes of a structure (e.g., [10, 11]), none of them, to the best of our knowledge, use techniques from topology design. It is now well known that dramatic reductions can be obtained by using topology rather than shape design. Indeed, we show that in almost all the examples that we consider, the reductions in amplitudes are more than an order of magnitude, and sometimes even close to two orders of magnitude.

Throughout this work, we only consider the minimization of vibrations of light fluid-loaded structures in the steady state, i.e., the state reached after the initial transients have died out due to the presence of damping. We also assume a linear vibration theory, so that the frequency of the response in the same as that of the driving frequency.

The organization of the remainder of the paper is as follows. In section 2, we motivate and define the global measure, namely, the dynamic compliance for a continuum structure. Using this definition, we formulate the topology optimization problem in section 3. The details of the formulation for the local measure, namely, the frequency response amplitude, are presented in section 4. Section 5 discusses the solution method, while section 6 presents some numerical examples to show the effectiveness of the formulations. The conclusions from this study are presented in section 7. In what follows, vectors are denoted by boldface small letters, and matrices are denoted by boldface capital letters.

2. THE DYNAMIC COMPLIANCE

To begin with, we define the dynamic compliance for a periodic load with only one excitation frequency, and later extend the definition to the case when the load is a superposition of several harmonics. The dynamic compliance that we propose is simply the average input power over a cycle. To motivate this definition, consider the simple one-dimensional equation of a mass–spring–dashpot system driven by a periodic force given by $f_0 \cos \hat{\omega} t$. The governing equation of this system is

$$m\ddot{x} + c\dot{x} + kx = f_0 \cos \hat{\omega} t,$$

where m is the mass, c is the damping constant, and k is the spring constant. Due to the presence of damping, the transients die out, and the steady state solution for the displacement and velocity is given by

$$x = A \cos(\hat{\omega} t - \alpha), \qquad \dot{x} = -\hat{\omega} A \sin(\hat{\omega} t - \alpha),$$

where α is the phase lag, and the amplitude, A, is given by

$$A = \frac{f_0}{\sqrt{(k - m\hat{\omega}^2)^2 + c^2\hat{\omega}^2}}.$$

Hence, the dynamic compliance is given by

$$\begin{aligned} J_d &= \frac{\hat{\omega}}{2\pi}\left[\int_0^{2\pi/\hat{\omega}} (f_0 \cos \hat{\omega} t)\, \dot{x}\, \mathrm{d}t\right] \\ &= -\frac{\hat{\omega}}{2\pi}\left[\int_0^{2\pi/\hat{\omega}} (f_0 \cos \hat{\omega} t)(\hat{\omega} A \sin(\hat{\omega} t - \alpha))\, \mathrm{d}t\right] \\ &= \tfrac{1}{2}\, \hat{\omega} A f_0 \sin \alpha \\ &= \frac{1}{2} \frac{\hat{\omega}^2 f_0^2 c}{[(k - m\hat{\omega}^2)^2 + c^2 \hat{\omega}^2]}. \end{aligned}$$

From the above expression, it is clear that the closer the system is to resonance, the higher is the dynamic compliance. Since $\hat{\omega}$ and f_0 are given, and assuming that c is also given, the values of k and m which minimize the above objective function (subject to some constraint) will automatically be such that the driving frequency $\hat{\omega}$ is "far" from the natural frequency $\omega_n = \sqrt{k/m}$.

For a continuum structure, the corresponding definition for the dynamic compliance (assuming that the prescribed displacement is zero) is

$$J_d = \frac{1}{T}\int_0^T \left[\int_{\Gamma_t} \bar{\mathbf{t}} \cdot \mathbf{v}\, \mathrm{d}\Gamma + \int_\Omega \mathbf{b} \cdot \mathbf{v}\, \mathrm{d}\Omega\right] \mathrm{d}t,$$

where $\mathbf{v}$ is the velocity field, $\mathbf{b} = \mathbf{b}_0 \cos \hat{\omega} t$ is the prescribed body force on Ω, $\bar{\mathbf{t}} = \bar{\mathbf{t}}_0 \cos \hat{\omega} t$ is the prescribed traction on Γ_t, and $T = 2\pi/\hat{\omega}$ is the time period. To see that this measure is positive definite in the purely mechanical theory that we are considering (i.e., when there is no heat input and heat conduction), consider the first law of thermodynamics

$$\frac{\mathrm{d}}{\mathrm{d}t}\int_\Omega \left(\frac{1}{2}\bar{\rho}\mathbf{v} \cdot \mathbf{v} + e\right) \mathrm{d}\Omega = \int_{\Gamma_t} \bar{\mathbf{t}} \cdot \mathbf{v}\, \mathrm{d}\Gamma + \int_\Omega \mathbf{b} \cdot \mathbf{v}\, \mathrm{d}\Omega,$$

where $\bar{\rho}$ is the density of the continuum, and e is the specific internal energy. Thus, for $\mathbf{v} \neq \mathbf{0}$

$$\begin{aligned} \int_0^T \left[\int_{\Gamma_t} \bar{\mathbf{t}} \cdot \mathbf{v}\, \mathrm{d}\Gamma + \int_\Omega \mathbf{b} \cdot \mathbf{v}\, \mathrm{d}\Omega\right] \mathrm{d}t &= \left[\int_\Omega \left(\frac{1}{2}\bar{\rho}\mathbf{v} \cdot \mathbf{v} + e\right) \mathrm{d}\Omega\right]_0^T \\ &= \left[\int_\Omega \mathrm{e}\, \mathrm{d}\Omega\right]_0^T \\ &> 0, \end{aligned}$$

since the kinetic energy has the same value at times 0 and T, and since the internal energy increases due to dissipation (the contribution to e due to the elastic strain energy, however, is the same at times 0 and T). Note that the value of J_d is zero if and only if $\mathbf{v} = \mathbf{0}$.

3. TOPOLOGY DESIGN FOR DYNAMIC COMPLIANCE MINIMIZATION

We are interested in finding a configuration of solids and void regions within a domain Ω that minimizes the dynamic compliance of the resulting structure, and such that the total

volume of material equals a specified volume $\bar{V}$. No restriction is placed on the connectedness of the solid part of Ω. We introduce the indicator function $\chi(\mathbf{x})$ given by

$$\chi(\mathbf{x}) = \begin{cases} 0 & \text{if } \mathbf{x} \in \Omega_v, \\ 1 & \text{if } \mathbf{x} \in \Omega_s, \end{cases} \tag{1}$$

where Ω_v and Ω_s denote the void and solid regions in Ω respectively. The volume of the structure is given by $\int_\Omega \chi(\mathbf{x})\,\mathrm{d}\Omega$, and the elasticity tensor at each point is $\mathbf{C} = \chi(\mathbf{x})\mathbf{C}_s$, where $\mathbf{C}_s$ is the elasticity tensor of the solid material.

We shall present the remaining formulation in the context of the finite element method. The details of the formulation of the finite element dynamic equations can be found, for example, in references [12–14]. The governing equations for the case when the loading is harmonic are given by

$$\mathbf{M}\ddot{\mathbf{u}} + \mathbf{C}\dot{\mathbf{u}} + \mathbf{K}\mathbf{u} = \mathbf{f}_0 \cos \hat{\omega} t,$$

where $\mathbf{u}$ is the displacement vector, $\mathbf{f}_0 \cos \hat{\omega} t$ is the periodic driving force vector, and $\mathbf{M}$, $\mathbf{C}$ and $\mathbf{K}$ are the mass, damping and stiffness matrices respectively. In order to solve the above set of equations for $\mathbf{u}$, we follow the usual strategy of solving

$$\mathbf{M}\ddot{\mathbf{x}} + \mathbf{C}\dot{\mathbf{x}} + \mathbf{K}\mathbf{x} = \mathbf{f}_0 \mathrm{e}^{\mathrm{i}\hat{\omega} t}$$

and taking $\mathbf{u}$ to be the real part of $\mathbf{x}$. Assuming $\mathbf{x}$ to be of the form $(\mathbf{x}_r + \mathrm{i}\mathbf{x}_s)\mathrm{e}^{\mathrm{i}\hat{\omega} t}$, and substituting into the above equation, we get

$$[\mathbf{K} - \hat{\omega}^2\mathbf{M} + \mathrm{i}\hat{\omega}\mathbf{C}](\mathbf{x}_r + \mathrm{i}\mathbf{x}_s) = \mathbf{f}_0. \tag{2}$$

Separating the real and imaginary parts, we get

$$(\mathbf{K} - \hat{\omega}^2\mathbf{M})\mathbf{x}_r - \hat{\omega}\mathbf{C}\mathbf{x}_s = \mathbf{f}_0, \tag{3}$$

$$(\mathbf{K} - \hat{\omega}^2\mathbf{M})\mathbf{x}_s - \hat{\omega}\mathbf{C}\mathbf{x}_r = \mathbf{0}. \tag{4}$$

From equation (4), we get

$$\mathbf{x}_r = -\frac{1}{\hat{\omega}}\,\mathbf{C}^{-1}(\mathbf{K} - \hat{\omega}^2\mathbf{M})\mathbf{x}_s, \tag{5}$$

which on substituting into equation (3) yields

$$\bar{\mathbf{K}}\mathbf{x}_s = -\hat{\omega}\mathbf{f}_0, \tag{6}$$

where

$$\bar{\mathbf{K}} = (\mathbf{K} - \hat{\omega}^2\mathbf{M})\mathbf{C}^{-1}(\mathbf{K} - \hat{\omega}^2\mathbf{M}) + \hat{\omega}^2\mathbf{C}. \tag{7}$$

Since $\mathbf{M}$, $\mathbf{C}$ and $\mathbf{K}$ are symmetric and positive definite, we see that the new "stiffness matrix", $\bar{\mathbf{K}}$, is also symmetric and positive definite. Hence, the problem of determining $\mathbf{x}_s$ can also be stated as a minimization of a "potential energy",† Π, where

$$\Pi(\mathbf{y}) = \tfrac{1}{2}\,\mathbf{y} \cdot \bar{\mathbf{K}}\mathbf{y} + \hat{\omega}\mathbf{y} \cdot \mathbf{f}_0.$$

†The reason for putting the terms stiffness matrix and potential energy in quotes is that their units are actually those of stiffness/time and power respectively. We use this terminology because of the obvious parallel which our problem has to a static compliance minimization problem.

At the solution $\mathbf{x}_s$, the value of Π is

$$\Pi(\mathbf{x}_s) = -\tfrac{1}{2}\,\mathbf{x}_s \cdot \bar{\mathbf{K}}\mathbf{x}_s.$$

As mentioned, the displacement vector $\mathbf{u}$ is given by the real part of $(\mathbf{x}_r + \mathrm{i}\mathbf{x}_s)\mathrm{e}^{\mathrm{i}\hat{\omega}t}$. Thus, the displacement and velocity vectors are given by

$$\mathbf{u} = (\cos\hat{\omega}t)\mathbf{x}_r - (\sin\hat{\omega}t)\mathbf{x}_s,$$

$$\mathbf{v} = -\hat{\omega}[(\sin\hat{\omega}t)\mathbf{x}_r + (\cos\hat{\omega}t)\mathbf{x}_s].$$

The dynamic compliance is given by

$$J_d = \frac{\hat{\omega}}{2\pi}\int_0^{2\pi/\hat{\omega}} (\mathbf{f}_0 \cos\hat{\omega}t)\cdot\mathbf{v}\,\mathrm{d}t$$

$$= -\tfrac{1}{2}\,\hat{\omega}\mathbf{f}_0 \cdot \mathbf{x}_s \tag{8}$$

$$= \tfrac{1}{2}\,\mathbf{x}_s \cdot \bar{\mathbf{K}}\mathbf{x}_s. \tag{9}$$

Thus, we have

$$J_d = -\Pi(\mathbf{x}_s).$$

The reason why we consider the dynamic compliance as a global measure of vibrations is evident from equation (9).

As is usually done, we convert our original discrete optimization problem to a continuous one by replacing the indicator function in equation (1) by the vector of continuous design variables, $\boldsymbol{\rho}$. Thus, we now write our optimization problem as: Find the vector of optimum design variables, $\boldsymbol{\rho}^*$, and the vector of associated "displacements", $\mathbf{x}_s$, that solves

$$\max_{\boldsymbol{\rho}} \min_{\mathbf{y}} \Pi(\boldsymbol{\rho}, \mathbf{y})$$

subject to appropriate constraints on the design variables. The inner subproblem in the above statement solves the problem of finding the "displacement", $\mathbf{x}_s$, for a given set of design variables, $\boldsymbol{\rho}$, while the outer subproblem solves the problem of minimizing the power input (or, alternatively, maximizing the "potential energy").

The vectors $\mathbf{x}_r$ and $\mathbf{x}_s$ can be found by directly solving equation (2) using a complex solver, or by solving equations (3) and (4), i.e.,

$$\begin{bmatrix} \mathbf{K} - \hat{\omega}^2\mathbf{M} & -\hat{\omega}\mathbf{C} \\ \hat{\omega}\mathbf{C} & \mathbf{K} - \hat{\omega}^2\mathbf{M} \end{bmatrix} \begin{bmatrix} \mathbf{x}_r \\ \mathbf{x}_s \end{bmatrix} = \begin{bmatrix} \mathbf{f}_0 \\ \mathbf{0} \end{bmatrix}.$$

Note that it is preferable to use the former strategy, both in terms of efficiency and storage, since the matrix in the above equation is neither symmetric nor banded. Once $\mathbf{x}_s$ is found, the objective function is found using equation (8).

The sensitivity of the objective function with respect to a design variable, ρ_i, can be found by using

$$\frac{\mathrm{d}\Pi}{\mathrm{d}\rho_i} = \frac{1}{2}\,\mathbf{x}_s \cdot \frac{\partial\bar{\mathbf{K}}}{\partial\rho_i}\mathbf{x}_s, \tag{10}$$

since $\partial \Pi / \partial \mathbf{y} = \mathbf{0}$ at the "equilibrium displacements", $\mathbf{x}_s$. To find the sensitivity in a more convenient form, we need to simplify equation (10). First note that since $\mathbf{C}^{-1}\mathbf{C} = \mathbf{I}$, we have

$$\frac{\partial \mathbf{C}^{-1}}{\partial \rho_i}\mathbf{C} + \mathbf{C}^{-1}\frac{\partial \mathbf{C}}{\partial \rho_i} = \mathbf{0},$$

which implies that

$$\frac{\partial \mathbf{C}^{-1}}{\partial \rho_i} = -\mathbf{C}^{-1}\frac{\partial \mathbf{C}}{\partial \rho_i}\mathbf{C}^{-1}. \tag{11}$$

Using the expression for $\bar{\mathbf{K}}$ given by equation (7) in conjunction with equation (11), we get

$$\frac{\partial \bar{\mathbf{K}}}{\partial \rho_i} = \frac{\partial}{\partial \rho_i}(\mathbf{K} - \hat{\omega}^2\mathbf{M})\mathbf{C}^{-1}(\mathbf{K} - \hat{\omega}^2\mathbf{M}) - (\mathbf{K} - \hat{\omega}^2\mathbf{M})\mathbf{C}^{-1}\frac{\partial \mathbf{C}}{\partial \rho_i}\mathbf{C}^{-1}(\mathbf{K} - \hat{\omega}^2\mathbf{M})$$

$$+ (\mathbf{K} - \hat{\omega}^2\mathbf{M})\mathbf{C}^{-1}\frac{\partial}{\partial \rho_i}(\mathbf{K} - \hat{\omega}^2\mathbf{M}) + \hat{\omega}^2\frac{\partial \mathbf{C}}{\partial \rho_i}.$$

Using equation (5), and the symmetry of $(\mathbf{K} - \hat{\omega}^2\mathbf{M})$ and $\mathbf{C}$, we have

$$\mathbf{x}_s \cdot \frac{\partial \bar{\mathbf{K}}}{\partial \rho_i}\mathbf{x}_s = \hat{\omega}^2\left[\mathbf{x}_s \cdot \frac{\partial \mathbf{C}}{\partial \rho_i}\mathbf{x}_s - \mathbf{x}_r \cdot \frac{\partial \mathbf{C}}{\partial \rho_i}\mathbf{x}_r\right] - 2\hat{\omega}\mathbf{x}_r \cdot \frac{\partial}{\partial \rho_i}(\mathbf{K} - \hat{\omega}^2\mathbf{M})\mathbf{x}_s.$$

Thus, the sensitivity of the objective function given by equation (10) can be written as

$$\frac{\mathrm{d}\Pi}{\mathrm{d}\rho_i} = \frac{\hat{\omega}^2}{2}\left[\mathbf{x}_s \cdot \frac{\partial \mathbf{C}}{\partial \rho_i}\mathbf{x}_s - \mathbf{x}_r \cdot \frac{\partial \mathbf{C}}{\partial \rho_i}\mathbf{x}_r\right] - \hat{\omega}\mathbf{x}_r \cdot \left(\frac{\partial \mathbf{K}}{\partial \rho_i} - \hat{\omega}^2\frac{\partial \mathbf{M}}{\partial \rho_i}\right)\mathbf{x}_s. \tag{12}$$

Note that once the finite element analysis has been conducted, the sensitivity computation is quite trivial due to the explicit expression given above. The sensitivity of the constraint (which will typically be an explicit function of the design variables) is also easily computed.

In reality, the driving force is a superposition of several harmonics, i.e.,

$$\mathbf{f} = \sum_{i=1}^{m} \mathbf{f}_i \cos \hat{\omega}_i t.$$

Due to the linear nature of the governing equations, the total displacement, $\mathbf{u}$, is obtained merely by superposing the displacement solutions for each loading component. The problem of determining $(\mathbf{x}_s)_i$ corresponding to each frequency component, $\hat{\omega}_i$, can be written as

$$\min_{\mathbf{y}_1, \mathbf{y}_2, \ldots, \mathbf{y}_m} \Pi(\mathbf{y}_1, \mathbf{y}_2, \ldots, \mathbf{y}_m),$$

where the potential energy functional is now given by

$$\Pi(\mathbf{y}_1, \mathbf{y}_2, \ldots, \mathbf{y}_m) = \sum_{i=1}^{m}\left[\frac{1}{2}\mathbf{y}_i \cdot \bar{\mathbf{K}}_i\mathbf{y}_i + \hat{\omega}_i\mathbf{y}_i \cdot \mathbf{f}_i\right].$$

We noted above that the total displacement can be obtained by superposing the displacement solutions corresponding to each frequency component. It is, however, not obvious that the overall dynamic compliance is the sum of the dynamic compliances

corresponding to each individual frequency. We now prove this. We need to consider two cases:

(1) The frequencies $\hat{\omega}_i$ are an integer multiple of some base frequency $\hat{\omega}_0$, i.e., $\hat{\omega}_i = n_i\hat{\omega}_0$, where n_i is an integer (e.g., all the $\hat{\omega}_i$ are rational numbers).
(2) It is not possible to express all the $\hat{\omega}_i$ in the above manner (e.g., $\hat{\omega}_1 = \sqrt{2}$ and $\hat{\omega}_2 = \sqrt{3}$.)

Since in the second case, the loading is *not* periodic, and also since each irrational number can be approximated arbitrarily closely by a rational one, we focus only on the first case. In this case, the driving force is periodic with a period of $T = 2\pi/\hat{\omega}_0$ since

$$\cos[\hat{\omega}_i(t + T)] = \cos(\hat{\omega}_i t + 2\pi n_i) = \cos\hat{\omega}_i t \quad \forall i.$$

Thus, the force in this case can be expressed as

$$\mathbf{f} = \sum_{i=1}^{m} \mathbf{f}_i \cos n_i\hat{\omega}_0 t. \tag{13}$$

Conversely, any periodic force can be approximated arbitrarily closely by a trigonometric polynomial of the form

$$\mathbf{f} = \mathbf{f}_0 + \sum_{n=1}^{N} (\mathbf{f}_n^{(1)} \cos n\hat{\omega}_0 t + \mathbf{f}_n^{(2)} \sin n\hat{\omega}_0 t),$$

where N is chosen large enough to get the required degree of accuracy. Since the term $\mathbf{f}_0$ does not contribute to the dynamic compliance, and since the dynamic compliance corresponding to $\cos n\hat{\omega}_0 t$ and $\sin n\hat{\omega}_0 t$ for any n is the same, it suffices to consider the forcing function given in equation (13).

The average power input over a cycle for this forcing function is

$$\begin{aligned} J_d &= \frac{\hat{\omega}_0}{2\pi} \int_0^{2\pi/\hat{\omega}_0} \mathbf{f}\cdot\mathbf{v}\,\mathrm{d}t \\ &= \frac{\hat{\omega}_0}{2\pi} \int_0^{2\pi/\hat{\omega}_0} \left[\sum_{i=1}^{m} \mathbf{f}_i \cos n_i\hat{\omega}_0 t\right] \cdot \left[\sum_{i=1}^{m} -\hat{\omega}_i[(\sin n_i\hat{\omega}_0 t)(\mathbf{x}_r)_i + (\cos n_i\hat{\omega}_0 t)(\mathbf{x}_s)_i]\right] \mathrm{d}t. \end{aligned}$$

Using the orthogonality of the sin and cos functions, i.e.,

$$\int_0^{2\pi/\hat{\omega}_0} (\cos m_i\hat{\omega}_0 t)(\cos n_i\hat{\omega}_0 t)\,\mathrm{d}t = \begin{cases} 0 & \text{if } m_i \neq n_i, \\ \pi/\hat{\omega}_0 & \text{if } m_i = n_i, \end{cases}$$

$$\int_0^{2\pi/\hat{\omega}_0} (\cos m_i\hat{\omega}_0 t)(\sin n_i\hat{\omega}_0 t)\,\mathrm{d}t = 0 \quad \forall m_i, n_i,$$

we get

$$\begin{aligned} J_d &= -\frac{1}{2}\sum_{i=1}^{m} \hat{\omega}_i \mathbf{f}_i \cdot (\mathbf{x}_s)_i \\ &= \sum_{i=1}^{m} \frac{1}{2}\bar{\mathbf{K}}_i(\mathbf{x}_s)_i \cdot (\mathbf{x}_s)_i. \end{aligned}$$

The dynamic compliance and the potential function are related as

$$J_d = -\Pi((\mathbf{x}_s)_1, (\mathbf{x}_s)_2, \ldots, (\mathbf{x}_s)_m).$$

From the above equations, the optimization problem for the case when the forcing function is a superposition of several harmonics, can be written as:
Find the vector of optimum design variables $\boldsymbol{\rho}^*$, and the vector of associated "displacements", $(\mathbf{x}_s)_i$, corresponding to each loading frequency $\hat{\omega}_i$, that solves

$$\max_{\boldsymbol{\rho}} \min_{\mathbf{y}_1, \mathbf{y}_2, \ldots, \mathbf{y}_m} \Pi(\boldsymbol{\rho}, \mathbf{y}_1, \mathbf{y}_2, \ldots, \mathbf{y}_m)$$

subject to appropriate constraints on the design variables. The sensitivity of the above objective function with respect to a design variable is obtained by superposing the sensitivities for each individual frequency as given by equation (12), i.e., if $(\mathrm{d}\Pi/\mathrm{d}\rho_i)_j$ denotes the sensitivity of the objective function corresponding to each frequency component $\hat{\omega}_j$, then

$$\frac{\mathrm{d}\Pi}{\mathrm{d}\rho_i} = \sum_{j=1}^{m} \left(\frac{\mathrm{d}\Pi}{\mathrm{d}\rho_i}\right)_j. \tag{14}$$

4. FREQUENCY RESPONSE AMPLITUDE MINIMIZATION

As discussed in the Introduction, although the dynamic compliance is a good measure for minimizing vibrations in a global or overall sense, in certain applications, one wants to minimize the vibration amplitude at a certain user-defined point in the structure. We now discuss this problem, again first considering the case of harmonic loading. In what follows, $\mathbf{z}$ denotes the quantity $\mathbf{x}_r + \mathrm{i}\mathbf{x}_s$, $\mathbf{a} \cdot \mathbf{b}$ denotes $\sum_i a_i b_i$, and the superscript "*" denotes the complex conjugate.

Let $\mathbf{q} = [0\ 0\ \ldots\ 1\ 0\ \ldots]$ be the vector with 1 at the degree of freedom (d.o.f.) where the amplitude of vibration, A, is to be minimized, and 0 elsewhere. Let $\alpha = \mathbf{q} \cdot \mathbf{z}$, $\alpha^* = \mathbf{q} \cdot \mathbf{z}^*$. Then we have

$$A^2 = \alpha^* \alpha. \tag{15}$$

To keep the form of the optimization problem similar to the dynamic compliance problem, we write it as:
Find the vector of optimum design variables, $\boldsymbol{\rho}^*$, that solves

$$\max_{\boldsymbol{\rho}} -A$$

subject to the equations of equilibrium and appropriate constraints on the design variables.

To compute the sensitivity of the objective function, $(-A)$, with respect to a design variable, ρ_i, we first compute $\mathrm{d}\alpha/\mathrm{d}\rho_i$. Differentiating (2), and using the fact that $\mathbf{f}_0$ and $\hat{\omega}$ are independent of ρ_i, we get

$$\frac{\mathrm{d}\mathbf{z}}{\mathrm{d}\rho_i} = -[\mathbf{K} - \hat{\omega}^2\mathbf{M} + \mathrm{i}\hat{\omega}\mathbf{C}]^{-1}\left[\left(\frac{\partial \mathbf{K}}{\partial \rho_i} - \hat{\omega}^2 \frac{\partial \mathbf{M}}{\partial \rho_i}\right) + \mathrm{i}\hat{\omega}\frac{\partial \mathbf{C}}{\partial \rho_i}\right]\mathbf{z}.$$

Since $\mathbf{q}$ is independent of ρ_i,

$$\frac{\mathrm{d}\alpha}{\mathrm{d}\rho_i} = -\,\mathbf{q}\cdot[\mathbf{K}-\hat{\omega}^2\mathbf{M}+\mathrm{i}\hat{\omega}\mathbf{C}]^{-1}\left[\left(\frac{\partial\mathbf{K}}{\partial\rho_i}-\hat{\omega}^2\frac{\partial\mathbf{M}}{\partial\rho_i}\right)+\mathrm{i}\hat{\omega}\frac{\partial\mathbf{C}}{\partial\rho_i}\right]\mathbf{z}. \tag{16}$$

Due to the symmetry of the $\mathbf{K}$, $\mathbf{M}$ and $\mathbf{C}$ matrices, we can write the above equation as

$$\frac{\mathrm{d}\alpha}{\mathrm{d}\rho_i} = -\,\mathbf{a}\cdot\mathbf{b}, \tag{17}$$

where

$$\mathbf{a} = [\mathbf{K}-\hat{\omega}^2\mathbf{M}+\mathrm{i}\hat{\omega}\mathbf{C}]^{-1}\,\mathbf{q},$$

$$\mathbf{b} = \left[\left(\frac{\partial\mathbf{K}}{\partial\rho_i}-\hat{\omega}^2\frac{\partial\mathbf{M}}{\partial\rho_i}\right)+\mathrm{i}\hat{\omega}\frac{\partial\mathbf{C}}{\partial\rho_i}\right]\mathbf{z}.$$

Note that computing the sensitivity using the expression given above is more efficient than computing it using (16) since $\mathbf{q}$ is a constant vector, and the factored complex stiffness matrix used in computing $\mathbf{z}$ can be used in computing $\mathbf{a}$ by treating $\mathbf{q}$ as a second load vector.

The sensitivity of A is obtained by differentiating both sides of (15):

$$\begin{aligned}
2A\frac{\mathrm{d}A}{\mathrm{d}\rho_i} &= \frac{\mathrm{d}\alpha^*}{\mathrm{d}\rho_i}\alpha+\alpha^*\frac{\mathrm{d}\alpha}{\mathrm{d}\rho_i}\\
&= \left(\frac{\mathrm{d}\alpha}{\mathrm{d}\rho_i}\right)^*\alpha+\alpha^*\frac{\mathrm{d}\alpha}{\mathrm{d}\rho_i}\\
&= 2\mathrm{Re}\left[\alpha^*\frac{\mathrm{d}\alpha}{\mathrm{d}\rho_i}\right]\\
&= -\,2\mathrm{Re}[\alpha^*(\mathbf{a}\cdot\mathbf{b})],
\end{aligned}$$

where Re denotes the real part of the argument, and the last step follows from (17). Thus, we have

$$-\frac{\mathrm{d}A}{\mathrm{d}\rho_i} = \frac{1}{A}\mathrm{Re}[\alpha^*(\mathbf{a}\cdot\mathbf{b})]. \tag{18}$$

Now, we consider the case when the driving force is given by equation (13). Although the total displacement can be obtained by superposing the displacement solutions corresponding to each frequency component, i.e.,

$$\mathbf{u} = \sum_{i=1}^{m}[\mathbf{cos}\,\hat{\omega}_i t(\mathbf{x}_r)_i-(\sin\hat{\omega}_i t)(\mathbf{x}_s)_i], \tag{19}$$

finding a closed-form expression for the maximum amplitude in general does not seem to be possible. Of course, at any point on the structure, one has the bound

$$A \leqslant \sum_{i=1}^{m} A_i,$$

where A is the maximum amplitude obtained from (19), and A_i is the amplitude corresponding to each load component, $\mathbf{f}_i \cos \hat{\omega}_i t$. A naive idea would be to try and minimize $\sum_{i=1}^{m} A_i$ in the hope that the actual amplitude, A, would also be reduced. But it is not hard to construct examples where $\sum_{i=1}^{m} A_i$ reduces, but A increases. Of course, if the minimum value of $\sum_{i=1}^{m} A_i$ is lower than the starting value of A then a reduction in the amplitude does result, though again it will, in general, not be the minimum amplitude possible. In view of this discussion, we shall, for the purpose of amplitude minimization, restrict overselves to the case of a harmonic driving force. Even if one were to assume $\sum_{i=1}^{m} A_i$ to be the objective function, the numerical scheme presented in the next section is valid; the sensitivity of the objective function required by the optimality criterion method is obtained simply by summing up the individual sensitivities given by (18).

5. SOLUTION METHOD

Since most of the noise in machinery is generated by the vibration of plate or shell structures, we present numerical examples for plate structures. We assume a uniform thickness h_i for each element i, and use the normalized quantities $\rho_i = h_i/h_{\max}$, where $h_{\max}$ is the maximum allowable thickness, as the set of design variables. However, we note that in the formulation there is *no restriction* on the choice of design variables. Other possible choices of design variables could be the magnitudes of lumped masses or springs attached at certain points on the domain, or the thickness and spacing of beam stiffeners attached to the plate or shell structure, and so on. The constraint that we impose is the volume constraint, i.e.,

$$V = \int_A h \, \mathrm{d}A \leqslant \bar{V}$$

where $\bar{V}$ is the specified volume.

While implementing a plate finite element model, care has to be taken that "locking" does not take place. We have implemented the MITC4 and MITC9 elements introduced by Bathe and co-workers (see Reference [12] and references therein) which are based on the Reissner–Mindlin plate model. The element stiffness matrix is given by

$$\mathbf{K}_e = \int_{-1}^{1} \int_{-1}^{1} (\mathbf{B}_\kappa^{\mathrm{T}} \mathbf{C}_b \mathbf{B}_\kappa + \mathbf{B}_\gamma^{\mathrm{T}} \mathbf{C}_s \mathbf{B}_\gamma) |\mathbf{J}| \, \mathrm{d}r \, \mathrm{d}s.$$

In the above equation, r and s denote natural co-ordinates, $|\mathbf{J}|$ is the determinant of the Jacobian matrix, $\mathbf{B}_\kappa$ and $\mathbf{B}_\gamma$ are the bending and transverse shear strain-displacement matrices, respectively, and $\mathbf{C}_b$ and $\mathbf{C}_s$ are given by

$$\mathbf{C}_b = \frac{Eh^3}{12(1-\nu^2)} \begin{bmatrix} 1 & \nu & 0 \\ \nu & 1 & 0 \\ 0 & 0 & \dfrac{1-\nu}{2} \end{bmatrix}, \qquad \mathbf{C}_s = \frac{Ehk}{2(1+\nu)} \begin{bmatrix} 1 & 0 \\ 0 & 1 \end{bmatrix},$$

where E is Young's modulus, ν is the Poisson ratio, k is the shear-correction factor (typically chosen as 5/6), and h is the thickness of the plate. The element mass matrix is given by

$$\mathbf{M}_e = \int_{-1}^{1} \int_{-1}^{1} \mathbf{N}^{\mathrm{t}} \mathbf{C}_m \mathbf{N} |\mathbf{J}| \, \mathrm{d}r \, \mathrm{d}s,$$

where $\mathbf{N}$ is the matrix of interpolation functions for the transverse displacement and rotations, and

$$\mathbf{C}_m = \begin{bmatrix} \bar{\rho}h & 0 & 0 \\ 0 & \dfrac{\bar{\rho}h^3}{12} & 0 \\ 0 & 0 & \dfrac{\bar{\rho}h^3}{12} \end{bmatrix},$$

where $\bar{\rho}$ denotes the density of material. From the above equations, it is clear that $\mathbf{K}$ and $\mathbf{M}$ depend on the thickness h only through the matrices $\mathbf{C}_b$, $\mathbf{C}_s$ and $\mathbf{C}_m$. Thus, the sensitivities $\partial\mathbf{K}/\partial\rho_i = h_{\max}\,\partial\mathbf{K}/\partial h_i$ and $\partial\mathbf{M}/\partial\rho_i = h_{\max}\,\partial\mathbf{M}/\partial h_i$ can be easily calculated.

We use the simple but widely used Rayleigh (or proportional) damping model where we assume

$$\mathbf{C} = \alpha\mathbf{M} + \beta\mathbf{K}.$$

We would like to emphasize that although we choose this model as an example, the choice of $\mathbf{C}$ in the formulation is completely general. The constants α and β are given by [13]

$$\alpha = \frac{2\omega_1\omega_2(\xi_1\omega_2 - \xi_2\omega_1)}{\omega_2^2 - \omega_1^2}, \qquad \beta = \frac{2(\xi_2\omega_2 - \xi_1\omega_1)}{\omega_2^2 - \omega_1^2},$$

where ξ_1 and ξ_2 are modal damping parameters corresponding to the two distinct modes with natural frequencies ω_1 and ω_2. One usually chooses ω_1 to be the lowest natural frequency (which ensures that $\mathbf{C}$ remains positive definite), and ω_2 to be the maximum frequency of interest in the loading or response. In our case, we choose ω_1 as mentioned above, and ω_2 as the smallest natural frequency greater than the biggest frequency component in the loading.

If one were to assume α and β as constant it would greatly simplify the sensitivity analysis. However, due to the dependence of these quantities on the natural frequencies, a more reasonable assumption, and one that we make for the numerical examples, is to assume the damping parameters ξ_1 and ξ_2 to be constant. However, the computational expense for finding the sensitivities of the damping matrix is considerably higher, since a generalized eigenvalue problem has to be solved at each iteration, as we now show.

The sensitivity of the damping matrix with respect to a typical design variable ρ_i is given by

$$\frac{\partial\mathbf{C}}{\partial\rho_i} = \alpha\frac{\partial\mathbf{M}}{\partial\rho_i} + \beta\frac{\partial\mathbf{K}}{\partial\rho_i} + \frac{\partial\alpha}{\partial\omega_j}\frac{\partial\omega_j}{\partial\rho_i}\mathbf{M} + \frac{\partial\beta}{\partial\omega_j}\frac{\partial\omega_j}{\partial\rho_i}\mathbf{K}, \tag{20}$$

where summation over j ranging from 1 to 2 is implied. The sensitivity computation of eigenvalues, both simple and repeated, is discussed in reference [15]; the sensitivity of a simple eigenvalue, ω_j, is given by

$$2\omega_j\frac{\partial\omega_j}{\partial\rho_i} = \phi_j^t\left[\frac{\partial\mathbf{K}}{\partial\rho_i} - \omega_j^2\frac{\partial\mathbf{M}}{\partial\rho_i}\right]\phi_j \quad \text{(no sum on } j\text{)},$$

where ϕ_j is the eigenvector corresponding to the natural frequency ω_j. Thus, we see that at least the first few eigenvalues and the corresponding eigenvectors need to be computed at

each iteration. Of course, computation of the eigenvalues and eigenvectors for a given design is an intrinsic part of any structural optimization strategy for dynamics problems, and is not a drawback of this particular technique. The cost of this computation can be significantly reduced if the eigensolver can use the eigenvalues and eigenvectors from the previous design iteration to iteratively solve the eigenproblem for the current design since the design perturbations are typically restricted to small values using move limits. One such iterative scheme is used by the package ARPACK [16]. Our experience was that there are significant savings in computational time using this strategy as compared to more conventional methods.

In lieu of an exact solution of the eigenproblem, one can use an approximate reanalysis procedure at each iteration; one such strategy is described by Chen [17]. Though this procedure works well for the first few iterations, the errors keep magnifying as the design iterations progress, and the approximate eigenvalues for the final converged design can be significantly different from the actual ones. Thus, although the approximate eigenvalues are "far" from the driving frequency at the end of the optimization process, some of the actual natural frequencies can be close to it! This is a danger that one has to be aware of while using any approximation technique for solving the eigenvalue problem. One other approximation that we tried is to compute α and β at the first iteration based on an eigenanalysis, and then maintain them constant for the subsequent iterations until the design converges, at which stage they are recomputed based on an eigenanalysis and used in the finite element analysis in order to get an accurate response. As already mentioned, maintaining α and β constant is not a good assumption, but the hope is that although the analysis might not be accurate at the intermediate stages, the topologies generated are still reasonably good. Our finding was that although this technique worked well for certain problems, it did not for some others; consequently, we do not use this approximation. Summarizing, we note that the example solutions presented in section 6 have been obtained without using any approximation technique for solving the eigenproblem, so that the results can act as benchmarks for any approximate techniques that are devised later.

Since the sensitivity of the objective function given by equation (14) or (18) can be negative, we use the modified optimality criterion method proposed by Ma *et al.* [9]. Using this method, the density update formula is given by

$$\rho_i^{k+1} = \left(\frac{\gamma_i + \mu \, \mathrm{d}V/\mathrm{d}\rho_i}{(\lambda + \mu)\, \mathrm{d}V/d\rho_i} \right)_k^{\eta} \rho_i^k \quad \text{for } \rho_{\min} \leqslant \rho_i^{k+1} \leqslant 1,$$

where γ_i is either $\mathrm{d}\Pi/\mathrm{d}\rho_i$ or $-\mathrm{d}A/\mathrm{d}\rho_i$ depending on whether dynamic compliance or amplitude minimization is being carried out, ρ_i^k stands for the design variable at the kth iteration, ρ_i^{k+1} is the updated design variable, η is a given parameter, and μ is a shift parameter chosen such that

$$\gamma_i + \mu \frac{\mathrm{d}V}{\mathrm{d}\rho_i} \geqslant 0 \quad \forall i.$$

For the dynamic compliance minimization, we get a value of $\eta = 1$. For the frequency amplitude minimization, we find that if one uses $\eta = 1$, there can be oscillation of the densities of some elements between two values. If one uses an extremely low value of η, then this problem of oscillation would be alleviated, but on the other hand, convergence can be quite slow; as a compromise, we use a value of $\eta = 0{\cdot}1$ in all our examples, and in addition reduce the move limits (see discussion below) whenever oscillations occur.

The Lagrange multiplier λ is found iteratively so as to satisfy the volume constraint. If the maximum change in density variables, $\Delta\rho_{max}$, is above a certain tolerance $\Delta\rho_{tol}$, then move limits are imposed by calculating the new density distribution as

$$(\boldsymbol{\rho})_{new}^{k+1} = \boldsymbol{\rho}^k + \frac{\Delta\rho_{tol}}{\Delta\rho_{max}}(\boldsymbol{\rho}^{k+1} - \boldsymbol{\rho}^k).$$

Note that since $\boldsymbol{\rho}^k$ and $\boldsymbol{\rho}^{k+1}$ satisfy the volume constraint, $(\boldsymbol{\rho})_{new}^{k+1}$ also automatically satisfies the volume constraint.

The optimization process is iterative. The required number of eigenvalues and eigenmodes for the starting design are computed. Then, equation (2) is solved using a complex solver to find $\mathbf{x}_r$ and $\mathbf{x}_s$. The eigenvalues, eigenvectors, $\mathbf{x}_r$ and $\mathbf{x}_s$ are used to find the sensitivity using equation (14) or (18). Subsequently, the modified optimality criterion method is used to find a new design. The above steps are repeated until the design converges.

6. NUMERICAL EXAMPLES

In this section, we present numerical examples to show the effectiveness of the proposed measures. There is a huge literature on optimization of structures with a view towards optimizing the acoustic response. Lamancusa [18] discusses various choices of design variables and objective functions that have been used—he concludes that acoustic power when used as an objective function produces the most consistently improved designs. Since the input power due to a periodic load on a structure is equal to the sum of the power dissipated in the structure and the acoustic power radiated to the surroundings, it is not obvious that redesigning the structure so as to minimize the dynamic compliance results in a reduction of the radiated sound power. However, strong numerical evidence has been presented in reference [19] to show that at least in the case of lightly loaded (i.e., where the effect of fluid loading can be neglected while analyzing the vibrations of the structure) baffled plates, the reduction obtained in the emitted sound power obtained by minimizing the dynamic compliance is almost as much as that obtained by minimizing the sound power directly. However, the great advantage is that, unlike previous approaches that try to carry out the optimization of the acoustic power directly, and hence need an acoustic analysis code, there is no need to conduct an acoustic analysis with the current strategy—the reductions in radiated sound power are obtained as an *indirect* benefit while minimizing the dynamic compliance. Thus, the current strategy could prove very cost effective from the view of reducing noise radiated from light-fluid loaded structures.

Although, we have implemented both the MITC4 and MITC9 plate elements, we present examples using only the MITC9 elements due to the unstable nature of lower-order elements (see reference [20] for a detailed analysis). Young's modulus, Poisson ratio and density are taken to be 210 GPa, 0·25 and 7800 kg/m^3 in all the examples. Black regions in the density plots represents a value of ρ_{max} (equal to 1), white regions represent a value of ρ_{min} (which we have chosen to be 0·1 in all examples), while grey regions represent intermediate densities. The value of ρ_{min} is chosen to be non-zero to prevent the mass, stiffness and damping matrices from becoming singular. The modal damping parameters are taken to be $\xi_1 = \xi_2 = 0{\cdot}01$.

Example 1 (*Cantilever beam*). The candidate domain, loading and boundary conditions are shown in Figure 1. The maximum allowable thickness is $h_{max} = 0{\cdot}5$ cm. The distributed load

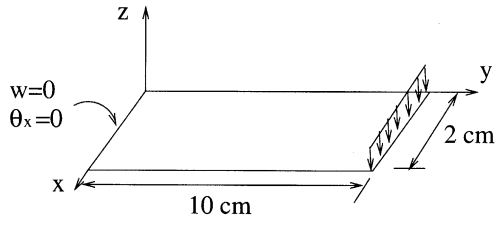

Figure 1. A cantilever beam subjected to end traction.

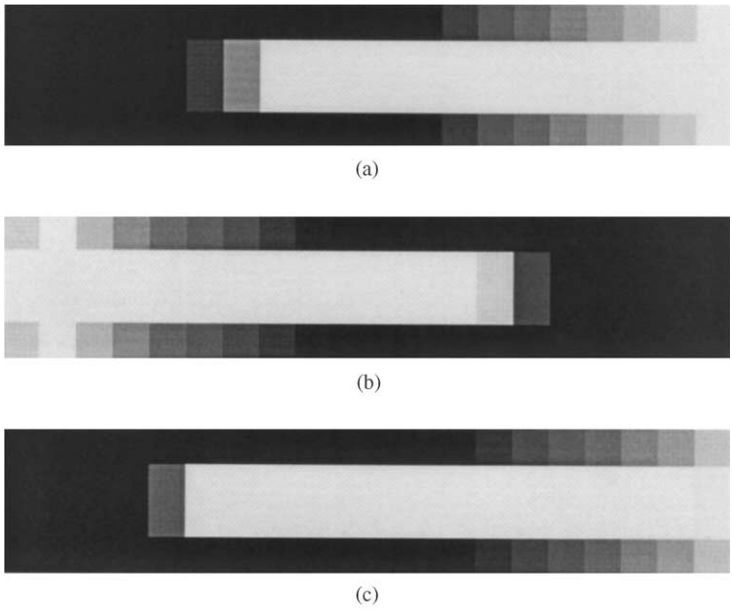

Figure 2. Density distribution for the cantilever beam example with dynamic compliance optimization in cases (a) and (b) and static compliance optimization in case (c): (a) $\hat{\omega} = 500$ rad/s, (b) $\hat{\omega} = 2500$ rad/s, (c) $\hat{\omega} = 0$ rad/s.

at the free edge is given by $1{\cdot}5 \cos \hat{\omega} t$ N/cm. Since both the geometry and loading are symmetric, we consider only half the domain for the analysis. A mesh of 20×2 MITC9 elements is used. $\Delta\rho_{tol}$ is taken to be 0·02. The specified volume fraction is 60%. Corresponding to this volume fraction, our starting design has a uniform thickness of 0·3 cm. The first three natural frequencies of the starting design obtained from the finite element model are 1589·8, 9918·1 and 27624·4 rad/s. We consider two cases:

(1) The driving frequency is less than the first natural frequency; we consider a value of $\hat{\omega} = 500$ rad/s.
(2) The driving frequency is more than the first natural frequency but less than the second natural frequency; we consider a value of $\hat{\omega} = 2500$ rad/s.

The resulting topologies are shown in Figure 2(a) and 2(b). The dynamic compliance reduces from $5{\cdot}93 \times 10^{-4}$ to $6{\cdot}03 \times 10^{-5}$ W in the first case, while it reduces from $5{\cdot}59 \times 10^{-3}$ to $1{\cdot}83 \times 10^{-4}$ W in the second case. The first three natural frequencies of the optimal topology shown in Figure 2(a) are 4416·7, 17 840 and 34 602·7 rad/s, while those for the

design in Figure 2(b) are 198, 8656 and 26 035 rad/s. Thus, as intended, the optimization strategy moves the natural frequencies of the structure away from the driving frequency in a very substantial way.

The topology in Figure 2(a) is almost the same as the optimal topology which minimizes the static compliance when a static distributed end load of 1·5 N/cm is applied (Figure 2(c)). Even though our definition of dynamic compliance does not reduce to the definition of the static compliance when $\hat{\omega} = 0$, the optimal topologies for driving frequencies $\hat{\omega} \to 0$ do result in statically stiff structures since at least the first few natural frequencies are driven towards higher values.

The designs corresponding to the three cases shown in Figure 2(a–c) for a refined mesh of density 40×4 are shown in Figure 3(a–c). The first three natural frequencies of the starting design are 1589·5, 9916 and 27 616·4 rad/s. For the first case, the dynamic compliance reduces from $5{\cdot}93 \times 10^{-4}$ to $5{\cdot}26 \times 10^{-5}$ W, while for the second one, it reduces from $5{\cdot}58 \times 10^{-3}$ to $1{\cdot}68 \times 10^{-4}$ W. The first three natural frequencies of the design in Figure 3(a) are 4634, 17 948 and 38 649 rad/s, while those for the design in Figure 3(b) are 179·9, 8611 and 26 939 rad/s. A comparison of Figures 2 and 3 seems to indicate that the dynamic problem is ill-posed just like its static counterpart; it can be made well-posed by adding a constraint on the perimeter [3].

As to a first approximation, the topologies in Figure 2(a) and 2(b) can be taken to be the tapered beams shown in Figure 4. Similar results for weight minimization of beam structures subject to stress constraints have been reported by Johnson [21]. When the first natural frequency is more than the driving frequency, the optimization process moves it away from the driving frequency thus producing a "stiff" structure as shown in Figure 4(a). On the other hand, in the second case, the optimization process moves the first natural frequency towards zero resulting in a structure which is statically speaking "flexible", but dynamically speaking "stiff" as shown in Figure 4(b). Johnson [21] provides the following physical explanation for this non-intuitive design—the increased tip thickness generates an

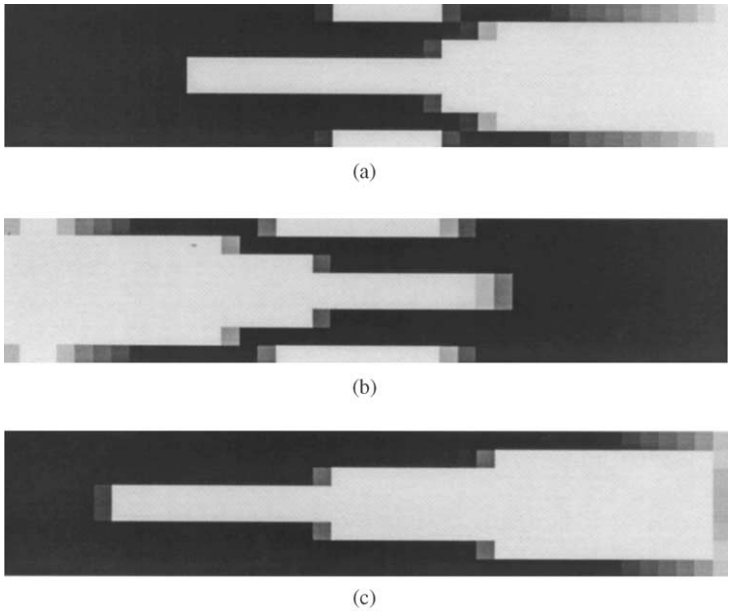

Figure 3. Density distribution for the cantilever beam example with the same data as in Figure 2, but with a refined mesh.

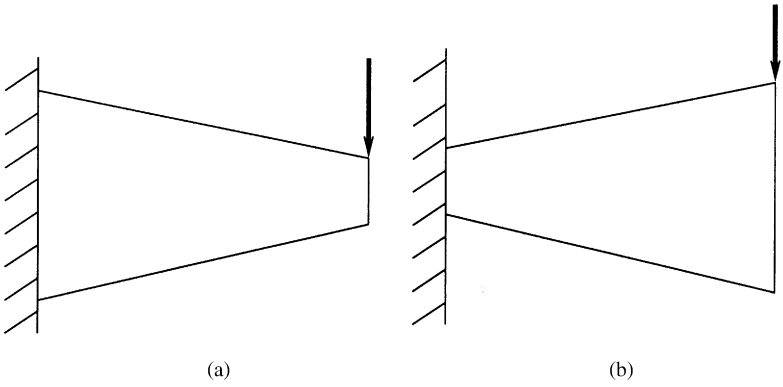

Figure 4. Approximation to the topologies in Figures 2(a) and 2(b).

inertial force that counteracts the driving force by acting out of phase with it, and thus relieves the stresses in the structure. In this case, one has to be careful to choose an appropriately high value of ρ_{min}, since, in a practical situation, the structure will pass briefly through resonance while the driving frequency is being increased from zero to its final value of 2500 rad/s. Note that our objective function is designed to reduce vibrations in the steady state, and care has to be taken that the structure does not fail in the transient stage preceding this steady state.

Since our strategy is gradient based, the optimum design (which is a local optimum) is strongly dependent on the choice of the starting design. Thus, with a choice of a beam of uniform thickness as the starting design when $\hat{\omega} = 2500$ rad/s, the optimization strategy leads us to the designs in Figures 2(b) and 3(b), which are statically speaking, flexible. Since this may be undesirable, one can first solve the static compliance optimization problem to generate the designs in Figures 2(c) and 3(c), and then use them as starting designs to minimize the dynamic compliance when $\hat{\omega} = 2500$ rad/s. In this manner, at least in some cases, it may be possible to get an optimum design that is "stiff" from both a static and dynamic viewpoint.

We now consider the minimization of the amplitude of vibration at the centre of the loaded end of the beam. For the sake of comparison of the optimum designs, we use the same starting design and meshes as in the dynamic compliance minimization case. The move limit, $\Delta\rho_{tol}$, is taken to be 0·01 and 0·02 for the coarse and fine mesh models, respectively. The converged topologies obtained using the coarse mesh when $\hat{\omega} = 500$ and $\hat{\omega} = 2500$ rad/s are shown in Figure 5(a) and 5(b) respectively. When $\hat{\omega} = 500$ rad/s, the amplitude reduces from a value of 0·1159 mm for the starting design to 0·03929 mm for the optimum design, while the first three natural frequencies for the optimal design are 3515·6, 17 746·7 and 43 208·6 rad/s. Again, we see that the optimization process moves the natural frequencies away from the driving frequency in a substantial way. With the dynamic compliance as the objective function, the amplitude reduces from 0·1159 to 0·0459 mm. As expected, the amplitude reduction is larger in the former case, albeit, only marginally. Although the difference is marginal in this particular case, we will see in the next case (when $\hat{\omega} = 2500$ rad/s) that it can be quite large.

For $\hat{\omega} = 2500$ rad/s, the amplitude of vibration reduces from $6{\cdot}575 \times 10^{-2}$ to $8{\cdot}03 \times 10^{-4}$ mm (a reduction by a factor of 80!) and 0·0216 mm (a reduction by a factor of 3), with the response amplitude and dynamic compliance as the objective functions respectively. The first three natural frequencies for the optimal design shown in Figure 5(b) are 221·4,

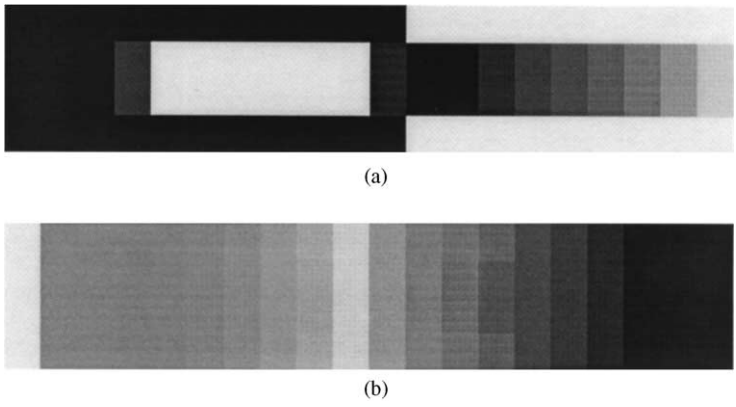

Figure 5. Density distribution for the cantilever beam example with frequency response amplitude optimization: (a) $\hat{\omega} = 500$ rad/s, (b) $\hat{\omega} = 2500$ rad/s.

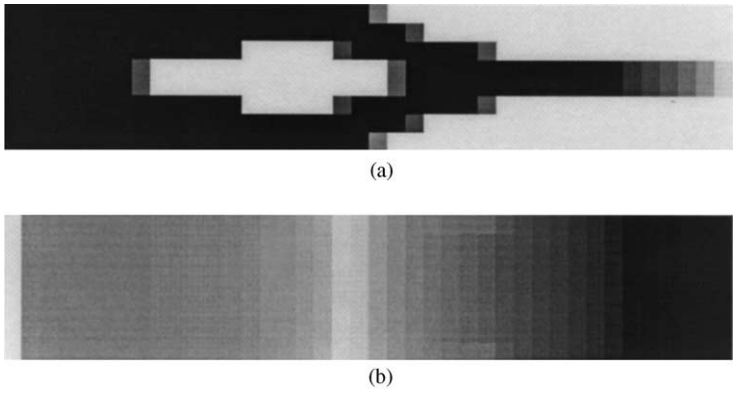

Figure 6. Density distribution for the cantilever beam example with the same data as in Figure 5, but with a refined mesh.

3426·8 and 18 626·3 rad/s. Now, we see that the first natural frequency is driven towards zero, while the second natural frequency approaches the driving frequency. Thus, the optimizer reduces the amplitude of vibration by modifying the starting design which vibrates predominantly in the first mode to a design which vibrates predominantly in the second mode. We would like to emphasize, however, that the dramatic reduction in amplitude at the end section is at the expense of an increased amplitude at other sections, e.g., the section midway between the two edges of the beam. Naturally, this does not happen with the dynamic compliance as the objective function; as can be seen from Figure 2(b), the struts at the edges of the beam prevent the amplitude at the midsection from increasing, which is consistent with the objective of reducting vibrations in an overall sense. Thus, as expected, and as pointed out in reference [19], the sound power reduction using the frequency response amplitude as the objective function is not as much as that obtained using the dynamic compliance. We note, however, that in certain aspects, the designs obtained with the amplitude and the dynamic compliance minimization strategies are similar; the designs in Figures 2(a) and 5(a) are from a static compliance viewpoint, stiff, while those in Figures 2(b) and 5(b) are flexible.

The optimal designs for the two load cases discussed above obtained using the refined mesh are shown in Figure 6(a) and 6(b). For $\hat{\omega} = 500$ rad/s, the amplitude of vibration

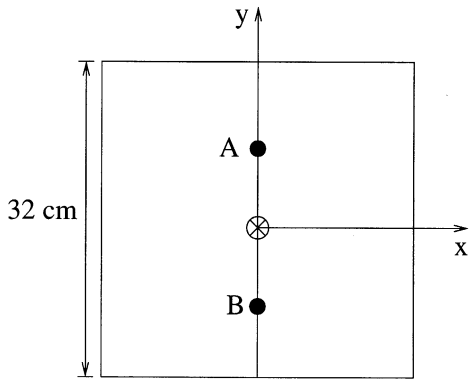

Figure 7. Domain and loading conditions for the plate example.

reduces from 0·11596 to 0·0351 mm, while for $\hat{\omega} = 2500$ rad/s, it reduces from $6{\cdot}572 \times 10^{-2}$ to $9{\cdot}07 \times 10^{-4}$ mm.

Example 2 (*Simply supported plate*). We consider a simply supported square plate of dimension 32 cm and $h_{max} = 1$ cm and loaded at the centre (see Figure 7). The specified volume fraction is 60%. Corresponding to this fraction, the starting design is taken to be a uniform plate of thickness 0·6 cm. Due to the symmetry of the structure and loading, we consider only a quarter of the plate for the analysis, and discretize it using an 8×8 uniform mesh of MITC9 elements. The first four natural frequencies are 1787·1, 8894·7, 8894·7 rad/s and 15 945·3 rad/s. We consider two cases:

(1) The load is given by $80 \cos 5000t$ N.
(2) The load is given by $80\ (\cos 5000t + \cos 15\,000t)$ N.

Choosing $\Delta\rho_{tol} = 0{\cdot}02$, the optimal topology for the first case is shown in Figure 8(a). There is a reduction of dynamic compliance from 0·0155 to $3{\cdot}43 \times 10^{-3}$ W. The first four natural frequencies of the optimal design are 893·4, 9749, 9758·4 and 12 827·6 rad/s. Note that the driving frequency moves the first and second natural frequencies away from it. The fourth natural frequency reduces from 15 945·3 to 12 827·6 rad/s in this case. However, in the second case, due to the frequency component of 15 000 rad/s in the loading, one would expect the fourth natural frequency to increase. The effect on the second and third natural frequencies is, however, unpredictable, since the 5000 and 15 000 rad/s components in the loading counteract each other. The first four natural frequencies of the optimal design for the second case shown in Figure 8(b) are 1347, 8095, 8513·5 and 22 462·2 rad/s. The dynamic compliance reduces from 0·253 W for the starting design to 0·0107 W for the optimal one. The optimal design under a static load of 80 N is shown in Figure 8(c). The corresponding results for a fine mesh with a 16×16 grid and $\Delta\rho_{tol} = 0{\cdot}04$ are shown in Figure 9. Note the similarity of the topologies in Figures 8 and 9.

For the frequency response optimization, we assume the load to be $80 \cos 5000t$ N, and consider two cases: (1) the amplitude of vibration is to be minimized at points A and B which lie midway between the point of loading and the top and bottom edges as shown in Figure 7, (2) the amplitude is to be minimized at point A alone. Due to the symmetry of the loading, geometry, and points at which the amplitude is to be minimized in the first case, we consider only a quarter of the plate for the analysis, and discretize it using first an 8×8 and then a 16×16 uniform mesh of MITC9 elements. We choose $\Delta\rho_{tol}$ to be 0·02 and 0·04 for the

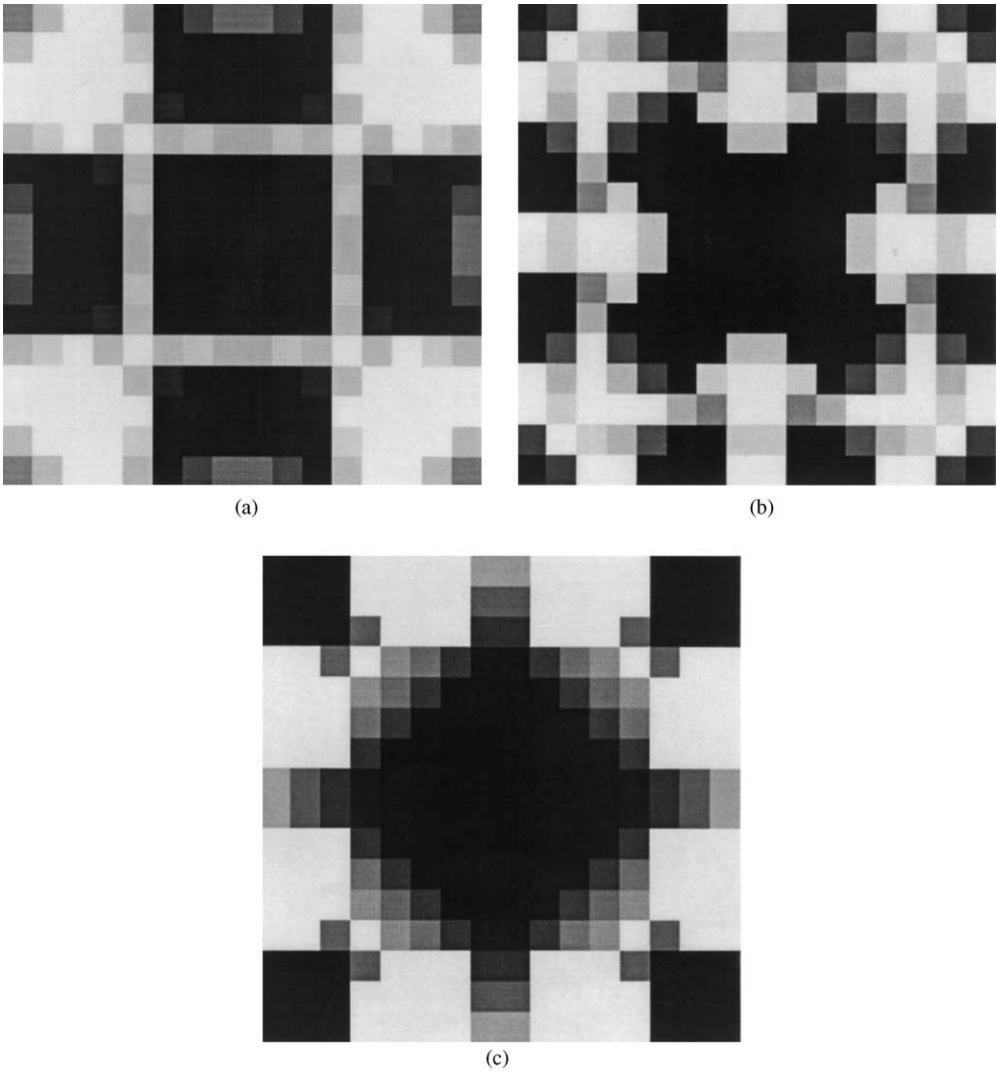

Figure 8. Density distribution for the simply supported plate example with dynamic compliance optimization in cases (a) and (b) and static compliance optimization in case (c): (a) $\hat{\omega} = 5000$ rad/s; (b) $\hat{\omega}_1 = 5000$ rad/s, $\hat{\omega}_2 = 15\,000$ rad/s; (c) $\hat{\omega} = 0$ rad/s.

coarse and fine mesh models respectively. The topologies obtained using the coarse and fine mesh for the first case are shown in Figure 10(a) and 10(b) respectively. In the coarse mesh model, the amplitude of vibration reduces from $2{\cdot}435 \times 10^{-3}$ to $6{\cdot}992 \times 10^{-5}$ mm while in the fine mesh one it reduces from $2{\cdot}4345 \times 10^{-3}$ to $8{\cdot}647 \times 10^{-5}$ mm, which is a reduction by a factor of about 30. However, at the point of loading, the amplitude *increases* from $5{\cdot}91 \times 10^{-4}$ to $3{\cdot}941 \times 10^{-3}$ mm, and from $6{\cdot}15 \times 10^{-4}$ to $5{\cdot}36 \times 10^{-3}$ mm in the coarse and fine mesh models respectively. Using the dynamic compliance as the objective function, the amplitude at points A and B in the coarse mesh model reduces from $2{\cdot}435 \times 10^{-3}$ to $1{\cdot}535 \times 10^{-3}$ mm which is not as dramatic a reduction as with the amplitude as objective function, but, as expected, at the point of loading, the amplitude *reduces* from $5{\cdot}91 \times 10^{-4}$ to $5{\cdot}50 \times 10^{-4}$ mm.

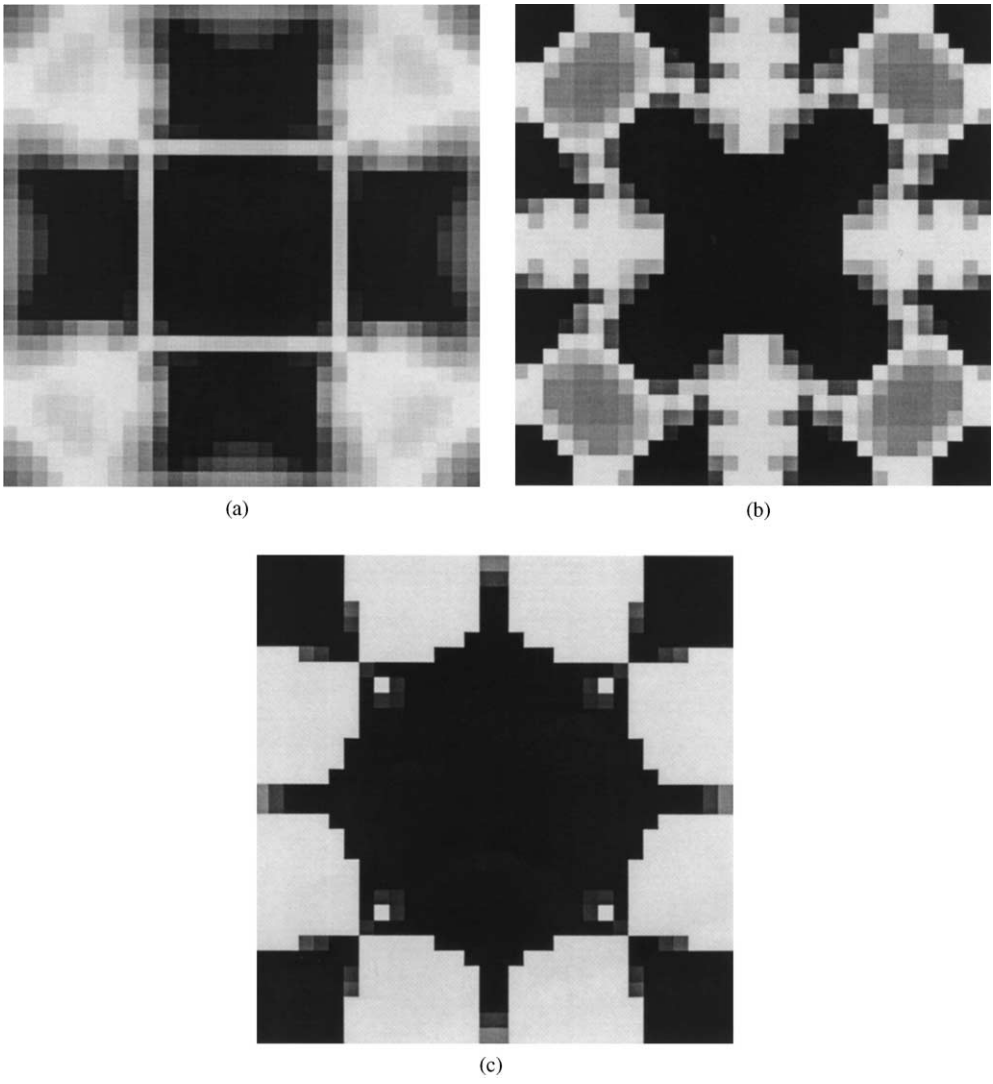

Figure 9. Density distribution for the simply supported plate example with the same data as in Figure 8, but with a refined mesh.

When amplitude minimization is desired at point A alone, we can no longer consider only a quarter of the plate for analysis, since the design can be unsymmetric with respect to the x-axis. However, we may still model only the right or left half of the plate in order to reduce the computational cost. Using the same mesh density as in the coarse mesh model above, we get the design shown in Figure 11. Since the constraint requiring that the amplitude at point B be minimized has been relaxed, one would expect the reduction in amplitude at point A to be more than in the case considered above. We indeed find this to be the case; the amplitude at A now reduces from $2{\cdot}435 \times 10^{-3}$ to $2{\cdot}630 \times 10^{-5}$ mm, which is a reduction by a factor of about 93.

From the topologies presented, it appears that the amplitude minimization problem results in predominantly "grey" optimal designs (i.e., large regions of the designs have intermediate densities), in contrast to the dynamic compliance problem which results in "black and white" topologies.

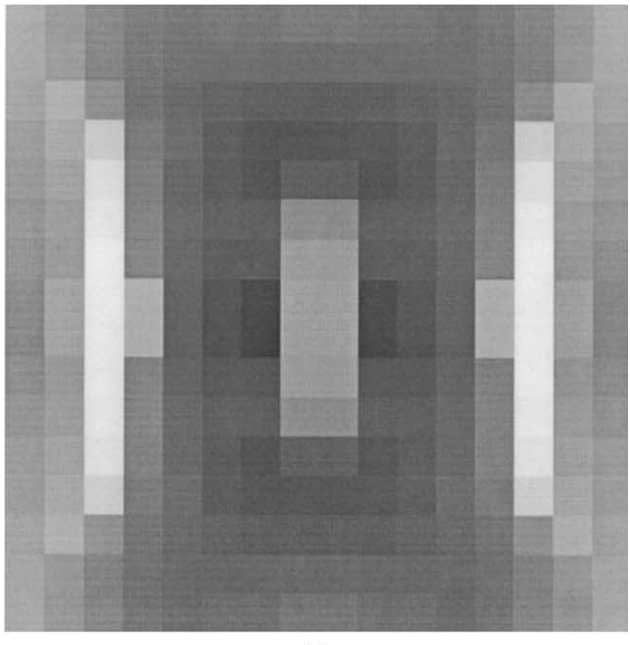

(a)

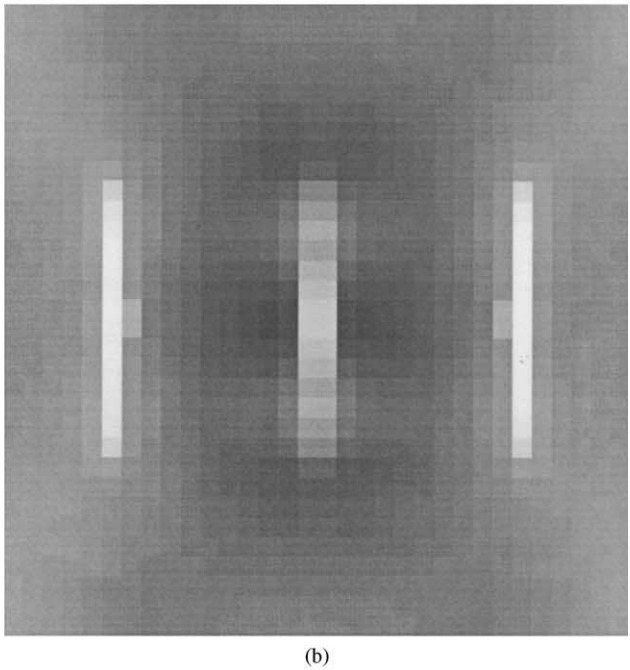

(b)

Figure 10. Density distribution for the plate example with $\hat{\omega} = 5000$ rad/s and amplitude minimization desired at points A and B: (a) coarse mesh, (b) fine mesh.

7. CONCLUSIONS

We have introduced a new measure for the "dynamic compliance", minimization of which reduces the vibrations of structures subjected to periodic loading in a global sense, and

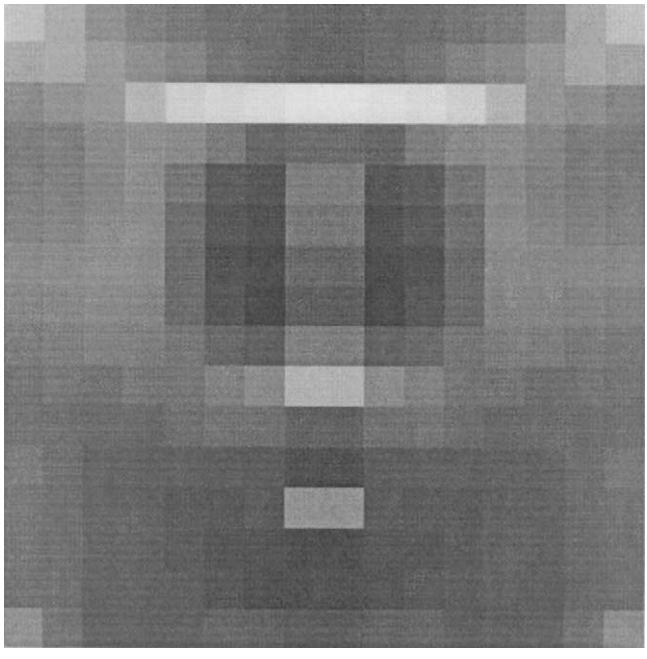

Figure 11. Density distribution for the plate example with $\hat{\omega} = 5000$ rad/s and amplitude minimization desired at point A alone.

hence which is likely to have implications from the viewpoint of noise reduction. The structure of the formulation is very similar to that of a static compliance minimization problem. We have also presented the topology design formulation for minimizing the frequency response amplitudes at a user-defined point in the structure. Due to the availability of analytical expressions for the sensitivities, the proposed optimization method for both measures is efficient. The numerical examples presented illustrate that, as intended, the measures are effective in reducing the vibrations in a global or local sense.

ACKNOWLEDGMENTS

The author gratefully acknowledges many helpful discussions with Professor C. S. Manohar of the Civil Engineering Department, Indian Institute of Science, and also gratefully acknowledges the partial financial support extended by the Naval Science and Technology Laboratory, Vishakhapatnam.

REFERENCES

1. G. ALLAIRE and R. V. KOHN 1993 *European Journal of Mechanics and Solids* **12**, 839–878. Optimal design for minimum weight and compliance in plane stress using microstructures.
2. M. P. BENDSØE and N. KIKUCHI 1988 *Computer Methods in Applied Mechanics and Engineering* **71**, 197–224.
3. M. P. BENDSØE 1995 *Optimization of Structural Topology, Shape and Material*. Berlin: Springer-Verlag.
4. C. S. JOG, R. B. HABER and M. P. BENDSØE 1994 *International Journal of Numerical Methods in Engineering* **37**, 1323–1350. Topology design with optimized self-adaptive materials.

5. M. P. BENDSØE and A. R. DIAZ 1994 *Structural Optimization* **7**, 138–140. Optimization of material properties for improved frequency response.
6. A. R. DIAZ and N. KIKUCHI 1992 *International Journal of Numerical Methods in Engineering* **35**, 1487–1502. Solutions to shape and topology eigenvalue optimization problems using a homogenization method.
7. L. A. KROG and N. OLHOFF 1999 *Computers and Structures* **72**, 535–563. Optimum topology and reinforcement design of disk and plate structures with multiple stiffness and eigenfrequency objectives.
8. Z. D. MA, N. KIKUCHI, H. C. CHENG and HAGIWARA 1995 *Transactions of the American Society of Mechanical Engineers Journal of Applied Mechanics* **62**, 200–207. Topological optimization technique for free vibration problems.
9. Z. D. MA, N. KIKUCHI and H. C. CHENG 1995 *Computer Methods in Applied Mechanics and Engineering* **121**, 259–280. Topological design for vibrating structures.
10. L. KITIS, B. P. WANG and W. D. PILKEY 1983 *Journal of Sound and Vibration* **89**, 559–569. Vibration reduction over a frequency range. A constraint function technique for improved structural dynamics.
11. D. WATTS and J. STARKEY 1990 *Transactions of the ASME*: *Journal of Vibration and Acoustics* **112**, 275–280. Design optimization of response amplitudes in viscously damped structures.
12. K. J. BATHE 1997 *Finite Element Procedures*. Englewood Cliffs, NJ: Prentice-Hall.
13. R. D. COOK, D. S. MALKUS and M. E. PLESHA 1989 *Concepts and Applications of Finite Element Analysis*. New York: John Wiley and Sons.
14. O. C. ZIENKIEWICZ and R. L. TAYLOR 1989 *The Finite Element Method*, Vol. 1, London: McGraw-Hill International Editions.
15. I. U. OJALVO 1986 *American Institute of Aeronautics and Astronautics Journal* **25**, 1386–1390. Efficient computation of mode-shape derivatives for large dynamic systems.
16. R. B. LEHOUCQ, D. C. SORENSEN and C. YANG 1998 *ARPACK User's Guide*: *Solution of Large-Scale Eigenvalue Problems with Implicity Restarted Arnoldi Methods*. Philadelphia: SIAM.
17. T. CHEN 1992 *International Journal of Numerical Methods in Engineering* **33**, 1927–1940. Optimum design of structures with both natural frequency and frequency response constraints.
18. J. S. LAMANCUSA 1993 *Computers and Structures* **48**, 661–675. Numerical optimization techniques for structural-acoustic design of rectangular plates.
19. C. S. JOG 2002 *IUTAM Symposium on Designing for Quietness*. Holland: Kluwer Academic Publishers. Reducing radiated sound power by minimizing the dynamic compliance, to appear.
20. C. S. JOG and R. B. HABER 1996 *Computer Methods in Applied Mechanics and Engineering* **130**, 203–226. Stability of finite element models for distributed-parameter optimization and topology design.
21. E. H. JOHNSON 1976 *American Institute of Aeronautics and Astronautics Journal* **14**, 259–261. Disjoint design spaces in the optimization of harmonically excited structures.